Springer

KSME

Journal of Mechanical Science and Technology 24 (4) (2010) 961~969
www.springerlink.com/content/1738-494x
DOI 10.1007/s12206-010-0211-0

Heat transfer and pressure drop amidst frost layer presence for the full geometry of fin-tube heat exchanger †

Sung-Jool Kim[1], Ho-Jin Choi[1], Man-Yeong Ha[1,*], Seok-Ro Kim[2] and Seon-Wook Bang[2]

[1]*School of Mechanical Engineering, Pusan National University, San 30, Jangjeon Dong, Geumjeong Gu, Busan 609-735, Korea*
[2]*Home Appliance Company, LG Electronics Inc., 391-2 Gaeum jeong-dong, Changwon City, Gyeongnam 641-711, Korea*

(Manuscript Received April 17, 2009; Revised October 1, 2009; Accepted January 21, 2010)

Abstract

The present study numerically solves the flow and thermal fields in the full geometry of heat exchanger modeling with frost layer presence on the heat exchanger surface. The effects of air inlet velocity, air inlet temperature, frost layer thickness, fin pitch, fin thickness, and heat exchanger shape on the thermo-hydraulic performance of a fin-tube heat exchanger are investigated. Heat transfer rate rises with increasing air inlet velocity and temperature, and decreasing frost layer thickness and fin pitch. Pressure drop rises with increasing air inlet velocity and frost layer thickness, and decreasing fin pitch. The effect of fin thickness on heat transfer and pressure drop is negligible. Based on the present results, we derived the correlations, which express pressure drop and temperature difference between air inlet and outlet as a function of air inlet velocity and temperature, as well as frost layer thickness.

Keywords: Fin-tube heat exchanger; Frost layer thickness; Fin pitch; Fin thickness; Air inlet velocity; Air inlet temperature

1. Introduction

Future energy systems will need to meet strengthened "globally agreed environmental regulations" in addition to offering reduced fuel consumption to cope effectively with global warming caused by climate change. Achieving such targets is a challenging task that requires the development of environment friendly energy systems. The demand for environment friendly energy systems has already initiated the search for novel technologies for power generation, transportation, home appliance, and renewable energy systems. To a large extent, success in developing highly efficient and clean energy systems depends on heat recovery technology that are applied to novel heat exchangers.

The performance of fin-tube heat exchangers used mainly in refrigerators and air conditioners depends on geometric design variables such as fin shape, fin and tube pitch, and the number of tube rows. Various air flow conditions, such as velocity, temperature, and humidity, are additional factors affecting performance. If the heat exchanger plays a role as an evaporator operating under the air temperature below the freezing point, heat exchanger performance is affected by the presence of frost layer formed on the surface of the heat exchanger. When on the surface, frost layers increases thermal resistance and air pressure drops across the heat exchanger, thus weakening overall performance [1]. Therefore, studying the effect of the frost layer on heat exchanger performance is important in the design of efficient heat exchangers.

Many researchers [2-14] have developed theoretical models based on heat and mass transfer between the air flow and frost layer, and have carried out experimental studies to investigate the performance of various heat exchangers under frosting conditions.

Some researchers [15-17] conducted CFD analysis for the simplified geometry of fin-tube heat exchangers with and without frost conditions to investigate in detail fluid flow and heat transfer characteristics of fin-tube heat exchangers.

Jang and Wu [15] numerically and experimentally studied fluid flow and heat transfer over a multi-row (1-6 rows) plate-fin and tube heat exchanger. They investigated the effects of different geometrical parameters, such as tube arrangement, tube row numbers, and fin pitch in order to obtain different Reynolds numbers ranging from 60 to 900. Their study showed that the number of tube rows achieved a minor effect on average heat transfer coefficient as the row numbers became greater than 4.

Romero-Me'ndez et al. [16] examined the influence of fin spacing on the over-tube side of a single-row fin-tube heat exchanger through flow visualization and numerical computation. Results showed that the Nusselt number was very small

† This paper was recommended for publication in revised form by Associate Editor Jun Sang Park

*Corresponding author. Tel.: +82 51 510 2440, Fax.: +82 51 515 3101
E-mail address: myha@pusan.ac.kr

in the wake region but increased when there was fluid exchange downstream.

Leu et al. [17] carried out numerical and experimental analyses to study heat transfer and flow in plate-fin and tube heat exchangers with inclined block shape vortex generators that are mounted behind the tubes. They investigated the effects of different span angles in detail to obtain a Reynolds number ranging from 400 to 3000.

Huang et al. [1] conducted a numerical study on the effect of frost layer thickness on heat transfer performance of a four-row plate finned tube heat exchanger both under constant air volume and variable air volume conditions. The effects of critical radius, surface roughness, frost thermal conductivity, and fan type on heat exchanger performance were also investigated.

Previous studies were all derived from theoretical models and employed CFD analysis for the simplified geometry of the fin-tube heat exchanger in the absence or presence of frost layer on the heat exchanger surface. However, few studies have been conducted on the full geometry of fin-tube heat exchanger having frost layer at the surface of the heat exchanger. Therefore, the purpose of the present study is to investigate the effect of air inlet velocity, air inlet temperature, frost layer thickness, fin pitch, fin thickness, and shape of heat exchanger on the thermo-hydraulic performance of the fin-tube heat exchanger. In this study, we considered the full geometry in the modeling of heat exchangers with frost layer formed at its surface. The correlations, which express pressure drop and temperature difference between air inlet and outlet as a function of air inlet velocity and temperature as well as frost layer thickness, are obtained and used as data for the virtual design of a refrigerator.

2. Numerical methodology

Figs. 1 and 2 show drawings of the full geometry of fin-tube heat exchangers that were considered in the present study. The first fin-tube heat exchanger (1st HX) shown in Fig. 1 is an evaporator in the freezer located at the bottom of the refrigerator, whereas the second fin-tube heat exchanger (2nd HX) shown in Fig. 2 is an evaporator in the freezer used in side-by-side refrigerators. The tubes in the 1st and 2nd HXs were arranged in a staggered manner. The tube diameter and longitudinal tube pitch for the 1st HX were 6.35 mm and 18 mm, respectively, while those for the 2nd HX were 8 mm and 30 mm, respectively. In consideration of the limited spaces available when we design these refrigerators, the width of the 1st HX is larger than its length and height whereas the height of the 2nd HX is larger than its width and length.

To numerically solve the flow and thermal fields in the 1st and 2nd HXs in relation to the presence of the frost layer, the following assumptions were made in the present study, which are similar to the assumptions offered by Huang et al. [1]:

(1) The flow is incompressible flow with constant properties and buoyancy force is neglected.

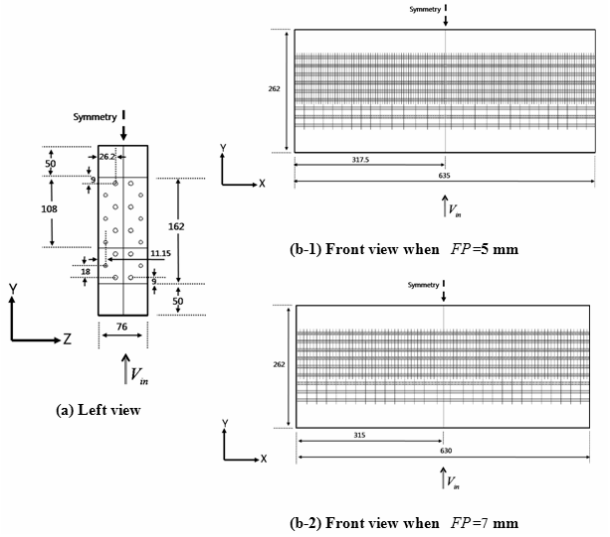

Fig. 1. Drawing of the full geometry of the 1st HX: (a) Left view, (b) Front view.

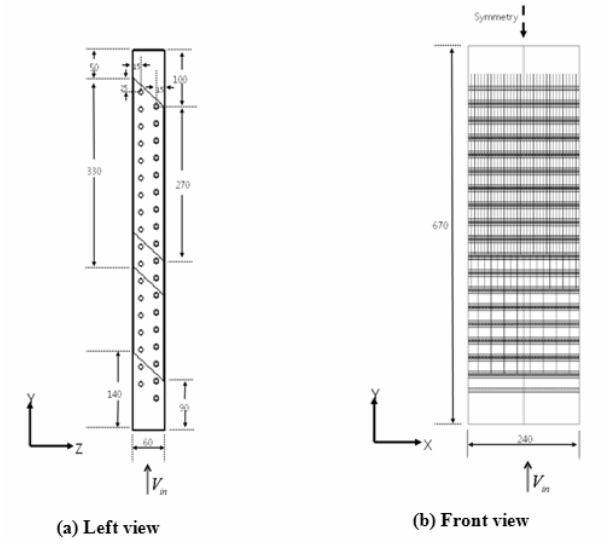

Fig. 2. Drawing of the full geometry of the 1st HX: (a) Left view, (b) Front view.

(2) Since the frost layer grows very slowly, the quasi-steady process is assumed in the present study.

(3) The frost layers that are formed on the fin and tube surfaces are homogeneous and have uniform thickness at a quasi-steady state.

(4) The heat inside the frost layer is transferred only via heat conduction and neglects mass transfer.

Under these assumptions, conservation equations were obtained on mass, momentum, and energy to solve the flow and thermal fields in the heat exchangers with frost layers on their surfaces. To solve closure problems of turbulence, the standard $k-\varepsilon$ model was used in the present calculation. To solve these highly non-linear conservation equations in order to govern the flow and thermal fields in the complex full ge-

ometries of frosted fin-tube heat exchangers, the commercial CFD code Fluent 6.3, a finite-volume based CFD package, was used. The central difference method was conducted to discretize the diffusion term, whereas the upwind difference method was used to discretize the convection term. The SIMPLE scheme was employed to obtain the solution during the iteration process. Numerical convergence criterion for the residuals of velocities, pressure, turbulence kinetic energy, and turbulent kinetic energy dissipation was 1×10^{-3}; for the residual of energy, it was 1×10^{-6}.

Compared with the entire size of the fin-tube heat exchangers, the size of fin pitch, fin thickness, and frost layer thickness were very small such that that it was difficult to efficiently generate the mesh. Fig. 3 shows the shape of the meshes generated in the tube, fin, and frost layer in the frosted 1st and 2nd HXs; the structured and unstructured grids were generated on the tube and fin surfaces, respectively. When the frost layers were formed on the tube and fin surfaces, the similar structured and unstructured grids were generated in the tube and fin frost layers, respectively. By following this grid generation method, we could efficiently generate the meshes in the frosted 1st and 2nd HXs, as shown in Fig. 3. When modeling and grid generation were conducted, a quarter of full geometry for the 1st HX and a half of full geometry for the 2nd HX were considered using the symmetric boundary condition. The number of meshes generated in the frosted 1st HX was about 740,000-1,210,000, whereas the number of grids in the frosted 2nd HX was about 780,000-1,530,000, depending on the frost layer thickness.

At the inlet, the Dirichlet boundary conditions for velocity and temperature were enforced. For the 1st HX, the air inlet velocities used were 0.1, 0.4, and 0.7 m/s, and air inlet temperatures used were 249, 255, and 261 K, which are the specifications suggested by the manufacturing company of the refrigerator. For the 2nd HX, air inlet velocities used were 1.0, 1.5, and 2.0 m/s, and air inlet temperatures were 252, 257, and 262 K. On the surfaces of the fin, tube, and frost layer, no-slip and no-penetration boundary conditions were imposed for the velocity field. For the temperature on the tube surface, an isothermal boundary condition of 242 K was enforced in the 1st HX, while an isothermal boundary condition of 243 K was used in the 2nd HX. For the fin and frost layer temperatures, the conduction equation, coupled with the air flow and air thermal fields, was solved. Table 1 shows the material properties of air, fin, and frost layer used in the present computation.

In the present study, we considered the effect of the frost layer thickness, fin pitch, and fin thickness on the performance of fin-tube heat exchangers, apart from the abovementioned effect of air inlet velocity and temperature. The frost layer thicknesses considered in the present study for the 1st and 2nd HXs were 0 (no frost thickness), 0.4, 0.8, and 1.2 mm. The fin pitches considered for the 1st HX were 5 and 7 mm, while that for the 2nd HX was 6 mm. The fin thickness considered for 1st HX was 0.2 mm; for 2nd HX, they were 0.16, 0.18, and 0.20 mm.

Table 1. Material properties of air, fin, and frost layer used in the present computation.

Properties	Fin	Frost	Air
Density (kg/m3)	2719	200	1.27
Specific heat (kJ/kg·K)	871	1980	1006.43
Thermal conductivity (W/m·K)	202.4	0.07	0.0242
Dynamic viscosity	-	-	$1.7*10^{-5}$

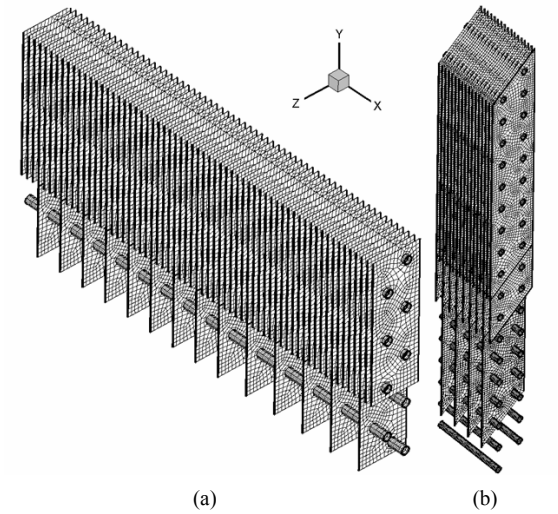

(a) (b)

Fig. 3. Shape of meshes generated in the tube, fin, and frost layer in the frosted layer of the frosted 1st and 2nd HXs.

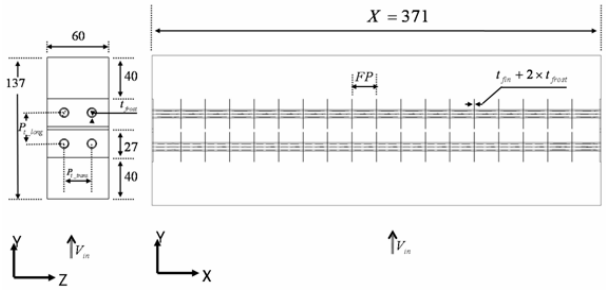

(a) (b)

Fig. 4. Geometry of fin-tube heat exchanger used in the experiment by Lee and Park [5] and Yang et al. [6]: (a) Left view, (b) Front view.

3. Results and discussion

To check the validity of the present computation, a CFD analysis of the geometry was conducted (Fig. 4), the same geometry used in the experiment by Lee and Park [5] and Yang et al. [6]. Table 2 shows the comparison between the present computational result for the air outlet temperature as a function of the frost layer thickness with the experimental data given by Lee and Park [5] and Yang et al. [6] for different thermal conductivities of frost layer (k_{frost}) of k_{frost} = 0.02, 0.07, and 0.13 W/m·K. When k_{frost} = 0.07 W/m·K, the computational results for the air outlet temperature of the present study well represents the experimental data given by Lee and Park [5] and Yang et al. [6]. Thus, we used 0.07 W/m·K as the

Table 2. Material properties of air, fin, and frost layer used in the present computation.

Frost thickness (mm)	Previous experimental results [5, 6]	Present results					
	Air outlet temp.	K_{frost} = 0.02 W/m·k		K_{frost} = 0.02 W/m·k		K_{frost} = 0.02 W/m·k	
		Air outlet temp.	Relative error (%)	Air outlet temp.	Relative error (%)	Air outlet temp.	Relative error (%)
0.4	2.87	3.80	32.5	2.91	1.3	2.68	6.7
0.8	3.48	4.51	29.6	3.26	6.3	2.83	18.6
1.2	3.56	4.94	38.7	3.53	0.9	2.97	16.6

Table 3. Grid spacing, sensible heat transfer rate based on the difference in the air inlet and outlet temperatures, and relative error between the heat transfer rates corresponding to the consecutive grid spacing. Table data allows for checking of the grid independency test in the computational results.

	X-axis					
Grid spacing (mm)	2	1.5	1.1	0.9	0.8	0.7
Heat transfer rate (W)	98.6	110.2	122.1	128.1	131.4	133.7
Relative error (%)	10.5	9.8	4.7	2.5	1.8	

	YZ-axis					
Grid spacing (mm)	4	3.5	3	2.5	2	1.8
Heat transfer rate (W)	128.6	129.4	133.7	134.5	136.0	138.1
Relative error (%)	1.3	1.2	1.1	1.1	1.0	

thermal conductivity of the frost layer in the present computation as mentioned in Table 1. Table 3 shows the grid spacing used, sensible heat transfer rate based on the difference in the air inlet and outlet temperatures, and relative error between the heat transfer rates corresponding to the consecutive grid spacing. The data in this table allows us to check the grid independency test in the computational results for the geometry shown in Fig. 4. When the grid spacing in the x-axis and y-z surface decreases, the relative error decreases. Thus, in the present study, 0.7 mm was employed for the grid spacing in the x-axis and 3 mm for the grid spacing in the y-z surface, in consideration of memory and computational time. As a result, we obtained the grid distribution for the 1st and 2nd HXs, as shown in Fig. 3.

Fig. 5 shows the distribution of velocities and isothermals along the y-direction at the cross-section close to the centerline of the 1st HX, with frost layer presence when fin pitch (FP) was 5 mm, air inlet velocity (V_{in}) was 0.7 m/s, and air inlet temperature (T_{in}) was 262 K. The distribution of flow and thermal fields shows the symmetric shapes around the center line between long fins. When the frost layer thickness increased, the velocity gradient increased gradually because the space between the fins diminished in size. The temperature

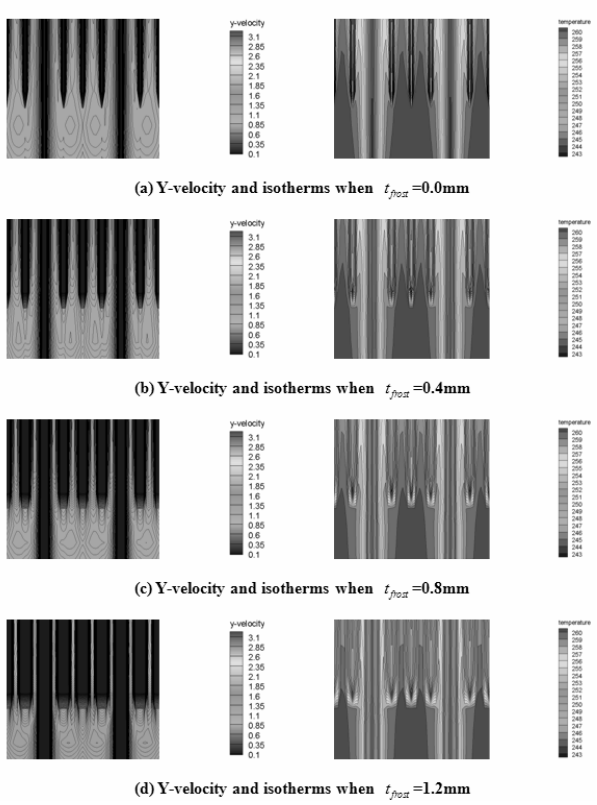

Fig. 5. Distribution of velocities and isothermals along the y-direction of the 1st HX with frost layer presence when FP = 5 mm, V_{in} = 0.7 m/s and T_{in} = 262 K.

gradient decreased gradually because heat transfer from fin to air was reduced in the presence of the frost layer. This phenomenon was caused by the decreasing air flow area and increasing thermal conduction resistance with increasing frost layer thickness.

Fig. 6 shows the 1st HX heat transfer rate as a function of frost layer thickness for different air inlet temperatures of T_{in} = 249, 255, and 261 K, and different fin pitches of FP = 5 and 7 mm when the inlet velocity was 0.7 m/s, and the temperature of tube (T_{tube}) was 242 K. When the frost layer thickness increased, the thermal resistance caused by the increment in the frost layer thickness increased as well, leading to a decrease in heat transfer rate. When air inlet temperature increased, the temperature difference between the air and the

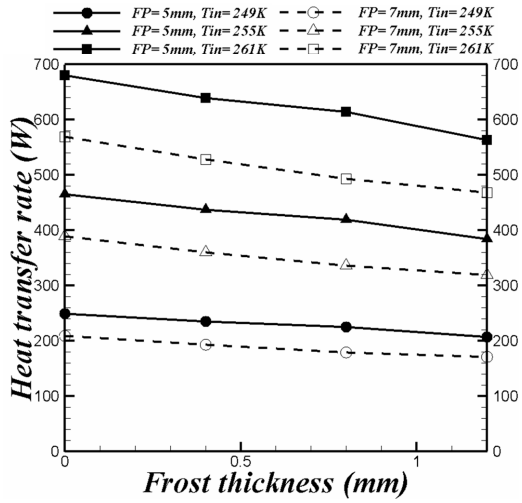

Fig. 6. Heat transfer rate of the 1st HX as a function of frost layer thickness for T_{in} = 249, 255, and 261 K, and FP = 5 and 7 mm when V_{in} = 0.7 m/s and T_{tube} = 242 K.

tube increased as well, causing a further increase in heat transfer rate.

When the fin pitch increased, the surface area of heat transfer decreased, such that the heat transfer rate was diminished under the same air inlet temperature. The heat transfer rate decreased almost linearly as a function of frost layer thickness for different air inlet temperatures and fin pitches.

The thermal resistance with frost layer consisting of R_{cond} and R_{conv} corresponding to the thermal resistance caused by the conduction R_{cond} and R_{conv} convection, respectively. To evaluate the relative magnitude of R_{cond} and R_{conv} in the heat exchanger with frost layer presence, we estimated the values of and as follows:

$$R_{cond} = \frac{t_{frost}}{k_{frost} A_s} \tag{1}$$

$$R_{cond} = \frac{1}{\bar{h} As} = \frac{(T_m - T_s)}{\dot{m} c_p (T_{in} - T_{out})} . \tag{2}$$

where t_{frost}, k_{frost}, and A_s are the thickness, thermal conductivity, and surface area of the frost layer forming on the heat exchanger surface, respectively. Meanwhile, $\bar{h}$, $\overline{T}_s$, $\dot{m}$, c_p, T_{in}, and T_{out} are the surface-averaged heat transfer coefficient, surface-averaged temperature of frost layer surface, mass flow rate of air, air specific heat, air inlet temperature, and air outlet temperature, respectively. In Eq. (2), $\overline{T}_m$ represents air mean temperature and is taken as a mean value of air inlet and outlet temperatures in the estimation of R_{cond} and R_{conv}.

R_{cond} and R_{conv} distribution obtained from Eqs. (1) and (2) is shown in Fig. 7 as a function of the frost layer thickness for V_{in} = 0.1, 0.4, and 0.7 m/s, and FP = 5 and 7 mm, when T_{in} = 261 K and T_{tube} = 242 K. R_{cond} increased linearly with increasing frost layer thickness irrespective of the magnitude

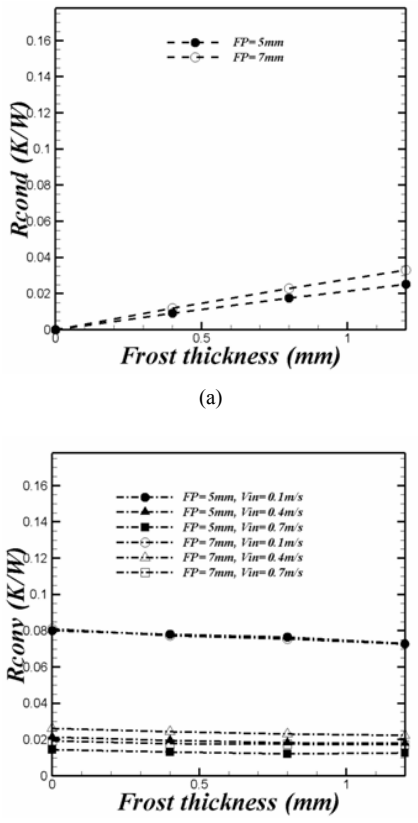

Fig. 7. Distribution of thermal resistance of the 1st HX as a function of the frost layer thickness for V_{in} = 0.1, 0.4 and 0.7 m/s, and FP = 5 and 7 mm when T_{in} = 261 K, and T_{tube} = 242 K, (a) R_{cond}, (b) R_{conv}.

of air inlet velocity. R_{cond} for FP = 5 mm was smaller compared with FP = 7 mm under the same frost layer thickness because the surface area of heat exchanger increased with decreasing fin pitch.

However, R_{conv} depends on air heat transfer coefficient (air flow velocity) and heat exchanger surface area with frost layer presence. When the air inlet velocity increased, the heat transfer coefficient increased as well, causing R_{conv} to decrease in the process, as shown in Eq. (2) and Fig. 7. With increasing air inlet velocity, the extent of increment in the heat transfer coefficient decreased gradually. As a result, the extent of decrement in R_{conv} decreased. With increasing frost layer thickness, R_{conv} decreased because of the diminishing distance between the frost layer and air flow velocity in the gap between the frost layers increased.

Fig. 8 shows the difference between air inlet and outlet temperatures (ΔT) and 1st HX heat transfer rate as a function of the frost layer thickness for different air inlet velocities of V_{in} = 0.1, 0.4, and 0.7 m/s, and different fin pitches of FP = 5 and 7 mm when the T_{in} = 261 K and T_{tube} = 242 K. When the inlet velocity was as low as V_{in} = 0.1 m/s, R_{conv} was much larger than R_{cond} (Fig. 7). As a result, heat transfer rate was affected mainly by R_{conv}. Thus, the extent of decrement in heat transfer rate as a function of the frost layer thickness

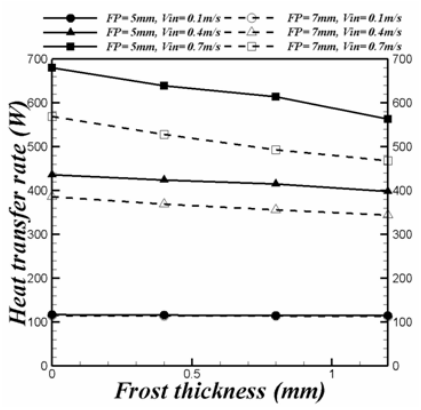

(a)

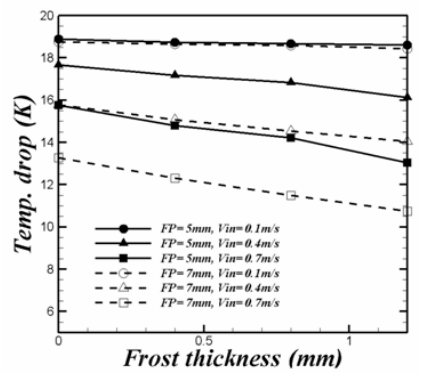

(b)

Fig. 8. Difference between air inlet and outlet temperatures and 1st HX heat transfer rate as a function of the frost layer thickness for V_{in} = 0.1, 0.4 and 0.7 m/s, and FP = 5 and 7 mm when T_{in} = 261 K and T_{tube} = 242 K.

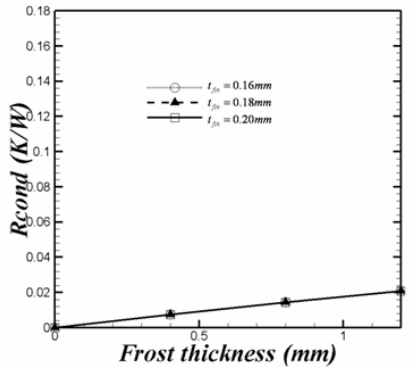

(a)

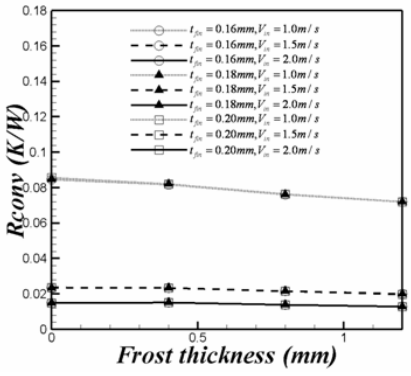

(b)

Fig. 9. Distribution of thermal resistance of the 2nd HX as a function of the frost layer thickness for V_{in} = 1.0, 1.5 and 2.0 m/s, and t_{fin} = 0.16, 0.18, and 0.20 mm when FP = 6 mm, T_{in} = 262 K, and T_{tube} = 243 K. (a) R_{cond}, (b) R_{conv}.

was slow for V_{in} = 0.1 m/s.

Since the residence time of air flow was large when V_{in} = 0.1 m/s, the drop in air outlet temperature was also huge due to sufficient residence time for heat transfer. Thus, ΔT for V_{in} = 0.1 m/s was relatively larger than that for V_{in} = 0.4 and 0.7 m/s, as shown in Fig. 8. However, even if the surface area increased with rising fin pitch from 5 mm to 7 mm at V_{in} = 0.1 m/s, both ΔT and heat transfer rates for different fin pitches of FP = 5 and 7 mm were independent on fin pitch, unlike in air flow residence time, producing a similar heat transfer rate for both cases (i.e., FP = 5 and 7 mm) at the low air inlet velocity of V_{in} = 0.1 m/s.

However, when the air inlet velocity was increased from 0.1 m/s to 0.4 and 0.7 m/s, R_{total} was diminished due to decreasing R_{conv}. Decreasing air flow residence time has leads to a decrease in ΔT. With increasing air inlet velocity, the extent of decrement in R_{total} was larger than in ΔT. As a result, the heat transfer rate, which occurred through the combined effects of R_{total} and ΔT, increased. If the fin pitch decreased from 7 mm to 5 mm at the high air inlet velocities of V_{in} = 0.4 and 0.7 m/s, the effect of increasing surface area with decreasing fin pitch on heat transfer rate would become larger than the decreasing residence time with increasing air inlet velocity. Thus, the heat transfer rate for FP = 5 mm was larger than that for FP = 7 mm at V_{in} = 0.4 and 0.7 m/s, and the difference in heat transfer rate between FP = 5 mm and FP = 7 mm increased with increasing air inlet velocity.

Fig. 9 shows the R_{cond} and R_{conv} distribution of 2nd HX as a function of the frost layer thickness for air inlet velocities of V_{in} = 1.0, 1.5, and 2.0 m/s, and for fin thicknesses of t_{fin} = 0.16, 0.18, and 0.20 mm, when FP = 6 mm, T_{in} = 262 K, and T_{tube} = 243 K. The figure enables us to see the effect of fin thickness on heat exchanger pressure drop and heat transfer rate. The variation of R_{cond} and R_{conv} as a function of the frost layer thickness for the 2nd HX (Fig. 9) was generally similar to that for the 1st HX shown (Fig. 7). As mentioned earlier, R_{cond} does not depend on the air inlet velocity but increases linearly with increasing frost layer thickness. Increasing air inlet velocity leads to R_{conv} decrease, and the R_{conv} decrement as a function of frost layer thickness was slow. The effect of fin thickness variation from 0.16 mm to 0.20 mm on R_{cond}, R_{conv}, and R_{total} was very minimal because the thermal conduction resistance in the fin was much smaller than that in the frost layer. Furthermore, the velocity variation in the gap between the frost layers was minimal.

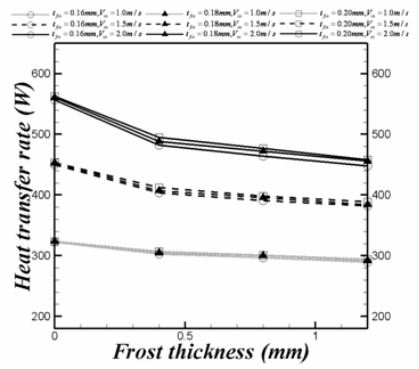

(a)

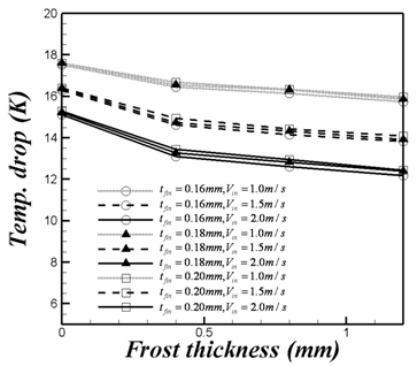

(b)

Fig. 10. Difference between air inlet and outlet temperature and the 2nd HX heat transfer rate as a function of the frost layer thickness for V_{in} = 1.0, 1.5 and 2.0 m/s, and t_{fin} = 0.16, 0.18, and 0.20 mm when FP = 6 mm, T_{in} = 262 K, and T_{tube} = 243 K.

Fig. 10 shows ΔT and heat transfer rate of 2nd HX as a function of the frost layer thickness for V_{in} = 1.0, 1.5, and 2.0 m/s, as well as t_{fin} = 0.16, 0.18, and 0.20 mm when FP = 6 mm, T_{in} = 262 K, and T_{tube} = 243 K. Similar to the case for the 1st HX shown in Fig. 10, the R_{total} for the 2nd HX increased with decreasing air inlet velocity and increasing frost layer thickness. Meanwhile, ΔT decreased due to decreasing residence time, as well as increasing air inlet velocity and frost layer thickness.

The heat transfer rate for 2nd HX obtained from the combined effect of R_{total} and ΔT increased with rising air inlet velocity, and decreased with increasing frost layer thickness. When fin thickness increased, heat transfer rate also increased due to increasing fin efficiency.

Fig. 11 shows 1st HX pressure drop as a function of air inlet velocity for different frost layer thicknesses of t_{frost} = 0.0, 0.4, 0.8, and 1.2 mm, and different fin pitches of FP = 5 and 7 mm. The pressure drop depended on the magnitude of air flow velocity in the gap between the frost layers. With increasing air inlet velocity, since air flow velocity in the gap between the frost layers increased, the pressure drop increased as well. The pressure drop of a heat exchanger is greatly affected by the blockage ratio, which is defined as $(t_{fin} + 2 \times t_{frost})/FP$. When frost layer thickness increased, the blockage ratio rose

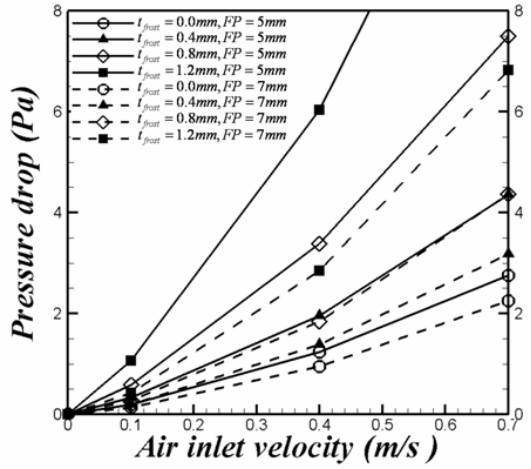

Fig. 11. Pressure drop of 1st HX as a function of air inlet velocity for t_{frost} = 0.0, 0.4, 0.8, and 1.2 mm, and FP = 5 and 7 mm when t_{fin} = 0.2 mm.

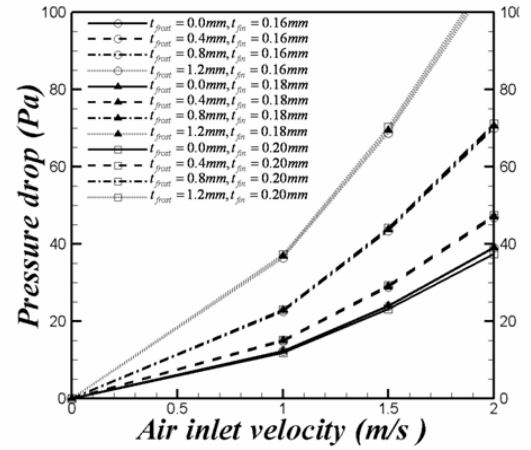

Fig. 12. Pressure drop of 2nd HX as a function of air inlet velocity for t_{frost} = 0.0, 0.4, 0.8, and 1.2 mm, and t_{fin} = 0.16, 0.18, and 0.20 mm when FP = 6 mm.

while the area of air flow in the gap between the frost layers decreased in proportion to the increasing frost layer thickness. As a result, with increasing frost layer thickness, the air flow velocity rose in proportion to the decreasing area of air flow while pressure drop increased.

If the fin pitch would decrease, the distance between the frost layers shrinks and the air flow velocity in the gap increases. In relation, the pressure drop increased with the rising fin pitch from 5 mm to 7 mm.

Fig. 12 shows the pressure drop for the 2nd HX as a function of air inlet velocity for different frost layer thicknesses of t_{frost} = 0.0, 0.4, 0.8, and 1.2 mm, as well as different fin thicknesses of t_{fin} = 0.16, 0.18, and 0.20 mm when FP = 6 mm. Similar to the 1st HX, the pressure drop for the 2nd HX increased with increasing air inlet velocity and frost layer thickness. However, for the three different fin thicknesses of t_{fin} = 0.16, 0.18, and 0.20 mm, the effect of fin thickness on the pressure drop was not large because the variation in the dis-

Table 4. The coefficients of ΔP and ΔT for the 1st HX when fin pitch are 5 mm and 7 mm; for the 2nd HX when fin thickness are 0.16, 0.18, and 0.20 mm.

	1st HX		2nd HX		
	Fin pitch = 5 mm	Fin pitch = 7 mm	Fin thickness = 0.16 mm	Fin thickness = 0.18 mm	Fin thickness = 0.20 mm
a_1	1.12114	0.39732	-	-	-
a_2	-1.84016	-0.61177	1.72157	1.72936	1.69967
a_3	2.56855	1.53624	0.022402	0.2686	0.71334
a_4	2.5311	2.48158	6.83561	6.90551	6.35324
b_1	0.18494	0.06424	0.2322	0.26395	0.54176
b_2	0.06188	-0.06386	2.08132	2.04301	0.78673
b_3	0.88471	0.52308	-	-	1.12572
b_4	1.81246	1.23681	6.21868	6.10153	6.53144
c_1	-	-	-	-	0.02949
c_2	0.00727	0.00359	-0.27653	-0.27259	-0.21933
c_3	-0.0055	-0.00476	-	-	-
c_4	-0.02142	-0.02118	0.74615	0.63219	-0.97271
d_1	-0.07955	-0.07441	-0.03331	-0.03187	-0.03024
d_2	-0.01614	-0.00498	-	-	-
d_3	-0.31805	-0.52222	-0.1112	-0.11131	-0.11766
d_4	1.03146	1.02641	1.0067	1.01165	1.02607
e_1	-2.89846	-2.4333	-0.99073	-0.95642	-0.92774
e_2	-0.22522	-0.05622	-	-	-
e_3	-9.63698	-16.3781	-3.66936	-3.64053	-3.68793
e_4	31.97912	31.96074	30.66847	30.78374	30.99397

tance between the frost layers was minimal.

Based on these results and using regression analysis via the SAS 8.2 software program, we derived the correlations, which expressed pressure drop ($\Delta P = P_{in} - P_{out}$) and temperature difference ($\Delta T = T_{in} - T_{out}$) between air inlet and outlet as a function of air inlet velocity and temperature, as well as frost layer thickness. The correlations of ΔP and ΔT from present computational results are defined as:

$$\begin{aligned}\Delta P = {} & V_{in}^2(a_1 t_{frost}^3 - a_2 t_{frost}^2 + a_3 t_{frost} + a_4) \\ & + V_{in}(b_1 t_{frost}^3 - b_2 t_{frost}^2 + b_3 t_{frost} + b_4) \\ & + (c_1 t_{frost}^3 - c_2 t_{frost}^2 + c_3 t_{frost} + c_4)\end{aligned} \quad (3)$$

$$\begin{aligned}\Delta T = {} & T_{in}(d_1 t_{frost} V_{in} + d_2 t_{frost} + d_3 V_{in} + d_4) \\ & + (e_1 t_{frost} V_{in} + e_2 t_{frost} + e_3 V_{in} + e_4)\end{aligned} . \quad (4)$$

The coefficients of ΔP and ΔT for the 1st HX when fin pitches were 5 mm and 7 mm, and for the 2nd HX when fin thicknesses were 0.16, 0.18, and 0.20 mm, are shown in Table 4.

The ΔP and ΔT obtained from the present correlations with the computational results from the present CFD analysis for the 1st and 2nd fin-tube heat exchangers were compared, providing a less than 1% error for ΔP and less than 5% for ΔT, respectively. These correlations are generally used when a refrigerator manufacturing company carries out the virtual design of a refrigerator.

4. Conclusion

CFD analysis for the full geometry of heat exchanger was employed to investigate the effect of the presence of frost layer on the heat exchanger surface on heat exchanger performance. This study considered the effect of air inlet velocity, air inlet temperature, frost layer thickness, fin pitch, and fin thickness on the heat transfer and pressure drop of two different heat exchangers.

Heat transfer rate increased with increasing air inlet velocity, decreasing frost layer thickness and fin pitch, and increasing air inlet temperature. Meanwhile, pressure drop increased with increasing air inlet velocity and frost layer thickness, and decreasing fin pitch. The effect of fin thickness on the heat transfer and pressure drop was negligible.

The correlations, which expressed pressure drop and temperature difference between air inlet and outlet as a function of air inlet velocity and temperature, as well as frost layer thickness, were obtained and used as data for the virtual design of a refrigerator.

Acknowledgment

This work was supported by the Korea Foundation for International Cooperation of Science & Technology (KICOS) through a grant provided by the Korean Ministry of Education, Science & Technology (MEST) in 2008 (No. K20702000013-07E0200-01310).

Nomenclature

A_s : Surface area of frost layer, m^2
c_p : Air specific heat, J/kg·K
FP : Fin pitch, mm
$\bar{h}$: Surface-averaged heat transfer coefficient, W/m2·K
k_{frost} : Thermal conductivity of frost layer, W/m·K
$\dot{m}$: Mass flow rate of air, kg/s
R_{cond} : Thermal resistance caused by conduction, K/W
R_{conv} : Thermal resistance caused by convection, K/W
R_{total} : Total thermal resistance, K/W
t_{fin} : Fin thickness, mm
t_{frost} : Frost layer thickness, mm
T_{in} : Air inlet temperature, K
$\bar{T}_m$: Air mean temperature, K
T_{out} : Air outlet temperature, K
$\bar{T}_s$: Surface-averaged temperature of frost layer surface,
T_{tube} : Tube temperature, K
V_{in} : Air inlet velocity, m/s
x,y,z : Cartesian coordinates

Sub/Superscripts

frost : Frost
fin : Fin
in : Inlet
out : Outlet
tube : Tube

References

[1] J. M. Huang, W. C. Hsieh, X. J. Ke and C. C. Wang, The effects of frost thickness on the heat transfer of finned tube heat exchanger subject to the combined influence of fan types, Appl. Thermal Eng. 28 (2008) 728-737.

[2] C. P. Tso, Y. C. Cheng and A. C. K. Lai, An improved model for predicting performance of finned tube heat exchanger under frosting condition, with frost thickness variation along fin, Appl. Thermal Eng. 26 (2006) 111-120.

[3] Y. Xia and A. M. Jacobi, Air-side data interpretation and performance analysis for heat exchangers with simultaneous heat and mass transfer: Wet and frosted surfaces, Int. J. Heat and Mass Transfer 47 (2005) 5089-5102.

[4] K. S. Lee, S. Jhee and D. K. Yang, Prediction of the frost formation on a cold flat surface, Int. J. Heat and Mass Transfer 46 (2003) 3789-3796.

[5] K. S. Lee and H. Y. Park, Study on the frost formation of fin-tube evaporator, LG Electronics Inc., 1st mid-term report (1993).

[6] D. K. Yang, K. S. Lee and S. Song, Modeling for predicting frosting behavior of a fin-tube heat exchanger, Int. J. Heat and Mass Transfer 49 (2006) 1472-1479.

[7] R. Yun, Y. Kim and M. Min, Modeling of frost growth and frost properties with airflow over a flat plate, Int. J. Refrig. 25 (2002) 362-371.

[8] H. Chen, L. Thomas and R. W. Besant, Fan supplied heat exchanger fin performance under frosting conditions, Int. J. Refrig. 26 (2003) 140-149.

[9] X. M. Wu and R. L. Webb, Investigation of the possibility of frost release from a cold surface, Exp. Thermal & Fluid Sci. 24 (2001) 151-159.

[10] D. K. Yang and K. S. Lee, Dimensionless correlations of frost properties on a cold plate, Int. J. Refrig. 27 (2004) 89-96.

[11] D. K. Yang and K. S. Lee, Modeling of frosting behaviour on a cold plate, Int. J. Refrig. 28 (2005) 396-402.

[12] Y. Xia, Y. Zhong, P. S. Hrnjak and A. M. Jacobi, Frost, defrost, and refrost and its impact on the air-side thermal-hydraulic performance of louvered-fin, flat-tube heat exchangers, Int. J. Refrig. 29 (2006) 1066-1079.

[13] D. B. Özkan and E. Özil, Experimental study on the effect of frost parameters on domestic refrigerator finned tube evaporator coils, Appl. Thermal Eng. 26 (2006) 2490-2493.

[14] C. C. Wang and K. Y. Chi, Heat transfer and friction characteristics of plain fin-and-tube heat exchangers, Part I: new experimental data, Int. J. Heat and Mass Transfer 43 (2000) 2681-2691.

[15] J. Y. Jang and M. C. Wu, Numerical and experimental studies of three-dimensional plate-fin and tube heat exchangers, Int. J. Heat and Mass Transfer 39 (1996) 3057-3066.

[16] R. R. Me′ndez, M. Sen, K. T. Yang and R. McClain, Effect of fin spacing on convection in a plate fin and tube heat exchanger, Int. J. Heat and Mass Transfer 43 (2000) 39-51.

[17] J. S. Leu, Y. H. Wu and J. Y. Jang, Heat transfer and fluid flow analysis in plate-fin and tube heat exchangers with a pair of block shape vortex generators, Int. J. Heat and Mass Transfer 47 (2004) 4327-4338.

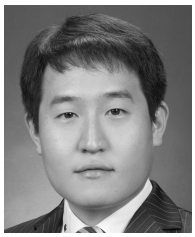

Sung-Jool Kim was born in Ulsan, Korea, in 1980. He received the B. S. and M. S. degrees in mechanical engineering from Pusan National University, in 2007 and 2009, respectively.

Man-Yeong Ha received his B.S. degree from Pusan National University, Korea, in 1981. He then received his M.S. and Ph.D. degrees from Korea Advanced Institute of Science and Technology, Korea and Pennsylvania State University, USA in 1983 and 1990, respectively. Dr. Ha is currently a Professor at the School of Mechanical Engineering at Pusan National University in Busan, Korea. He serves as an Editor of the Journal of Mechanical Science and Technology. Dr. Ha's research interests include thermal management, computational fluid dynamics, and micro/nano fluidics.